Magnetically Assisted Resistance Spot Welding of Dual-Phase Steel

The mode and intensity of an externally applied constant magnetic field were analyzed along with the effect on nugget formation

BY Y. B. LI, Y. T. LI, Q. SHEN, AND Z. Q. LIN

ABSTRACT

External magnetic field (EMF) has been verified as an effective way to improve the welding of dual-phase (DP) steels. In the present study, two typical modes of EMFs generated by, respectively, a single and a pair of permanent magnets, were used to study the magnetically assisted resistance spot welding (MA-RSW) process. Effects of the EMF mode and intensity on nugget formation were discussed on 0.80-mm-thick DP980 steel for the first time. Concerning the practical application, sensitivity of the MA-RSW process to welding current and the weldability of the MA-RSW process were experimentally investigated. Results showed that the horizontal component of the EMF magnetic flux increased monotonically from the center to the edge of the welding region. Due to the superposition of two symmetric magnetic fields, the horizontal magnetic flux density and the circumferential magnetic force under a pair of permanent magnets were, respectively, twice and 1.5 times that under a single one. Moreover, the diameter growth rate of the weld nugget was faster, the nugget symmetry better, and the macrocrystallization direction in the fusion less obvious. Meanwhile, with the increase in EMF intensity, the nugget diameter got larger, and the central thickness got thinner. Under the action of the EMF, weld tensile-shear strength, ductility, and fracture modes were all improved. Besides, such improvement was more obvious for welds under relatively low welding current. Moreover, the weld lobe diagram moved leftward by approximately 400 A under the EMF, while the overall width remained almost unchanged.

Introduction

Nowadays, resistance spot welding (RSW) is still the major joining technology used in car body assembly lines. On the other hand, in order to reduce body weight under the prerequisite of occupant safety, advanced high-strength steels (AHSS) with high strength-to-weight ratio have been gradually introduced into the structural component fabrications to replace the traditionally used mild steels (Ref. 1). Dual-phase (DP) steel, as one of the most common AHSS used in car body manufacturing, features both high strength and acceptable ductility owing to its unique microstructure, i.e., soft ferrite matrix with dispersed martensites at the grain boundaries (Ref. 2). Differing from the conventional mild steels, DP steel contains a relatively higher amount of carbon and alloy elements, which makes it much easier to form coarse martensite microstructures in the weld nugget (Refs. 3, 4).

Previous studies have demonstrated that these hard and brittle nonuniform microstructures might lead to a decrease in weld ductility and raise the risk of interfacial fracture (Refs. 3, 5). Such phenomenon is more severe in high-strength DP steels like DP980 (Ref. 6). Generally, button-pullout fracture is the preferred failure mode rather than interfacial fracture for its stronger capacity of energy absorption (Refs. 7, 8). Applying a posttempering process (Refs. 9, 10), reducing cooling rate (Ref. 11), or pretreating the workpieces by coating a layer of carbon dilution on the interface of the two steel sheets (Ref. 10) will refine these microstructures and be able to improve weld ductility. Nevertheless, these methods either reduce production efficiency or substantially raise production cost.

On the other hand, since nugget diameter is generally acknowledged as the major quality criterion for spot welds (Ref. 12) and the primary factor influencing the type of weld fracture (Ref. 13), some related studies (Refs. 6, 13) have tried to identify the minimum critical value of nugget diameter for button-pullout fracture with DP steels. At present, raising welding current is the most popular and most efficient method used in car body as-

KEYWORDS

Resistance Spot Welding (RSW)
Dual-Phase (DP) Steel
External Magnetic Field (EMF)
Electromagnetic Stirring
Grain Refinement

Y. B. LI (yongbinglee@sjtu.edu.cn), *Y. T. LI, Q. SHEN, and Z. Q. LIN are with the Shanghai Key Laboratory of Digital Manufacture for Thin-Walled Structures, Shanghai Jiao Tong University, Shanghai, China. LI and LIN are also with the State Key Laboratory of Mechanical System and Vibration, Shanghai Jiao Tong University, Shanghai, China.*

sembly lines to increase nugget diameter and ensure the overall weld quality. However, strong welding current usually consumes more energy and accelerates the electrode wear rate, which will eventually raise the total production cost.

In the past decades, as a simple, efficient, and low-cost technology, the magnetically assisted (MA) method has been successfully applied to continuous casting (Ref. 14), arc welding (Ref. 15), and other materials-processing technologies to control the melting and solidification of metals in specific processes. Earlier studies (Refs. 14, 15) have demonstrated that the MA method is capable of refining grain structures, reducing segregations and cracks, and improving mechanical performance of processed metals. Based on those studies, the magnetically assisted RSW process (MA-RSW) has recently been proposed to improve the weld quality of DP steels by applying an external magnetic field (EMF), which is produced by a pair of cylindrical magnets symmetrically mounted on the two electrode arms.

Latest research (Refs. 16–18) has demonstrated that compared with the traditional resistance spot welds (thereafter abbreviated as traditional weld), the magnetically assisted spot welds (MA weld) feature higher strength, better ductility, and longer fatigue life. However, the MA-RSW process is still an emerging topic, and the related studies, especially on magnetic field distribution and its practical effectiveness on high-strength DP steels are still unknown.

The present study was aimed to give a deeper understanding of the MA-RSW process. In this paper, a finite element (FE) model was proposed to investigate the effect of two different modes of EMF on the MA-RSW process. Nugget formations under the two modes were experimentally studied on 0.80-mm-thick DP980 steel in terms of nugget shape and microstructures. Trends of nugget size variations along with the changes in the EMF intensity were also revealed. Furthermore, effectiveness of the MA-RSW process was systematically discussed in terms of weld tensile-shear strength and weld lobe diagram.

Finite Element Model and Experimental Setup

Calculation Model and Boundary Conditions

Numerical simulations were carried out based on commercial FE code Ansys 11.0/multiphysics. In view of the symmetry features of a typical RSW process (Ref. 12), as shown in Fig. 1, a 1/2 2D axisymmetric submodel meshed with element PLANE 67 was used for electric field analysis and an 18-deg, 3D wedge-shaped submodel meshed with element SOLID 97 for magnetic field analysis.

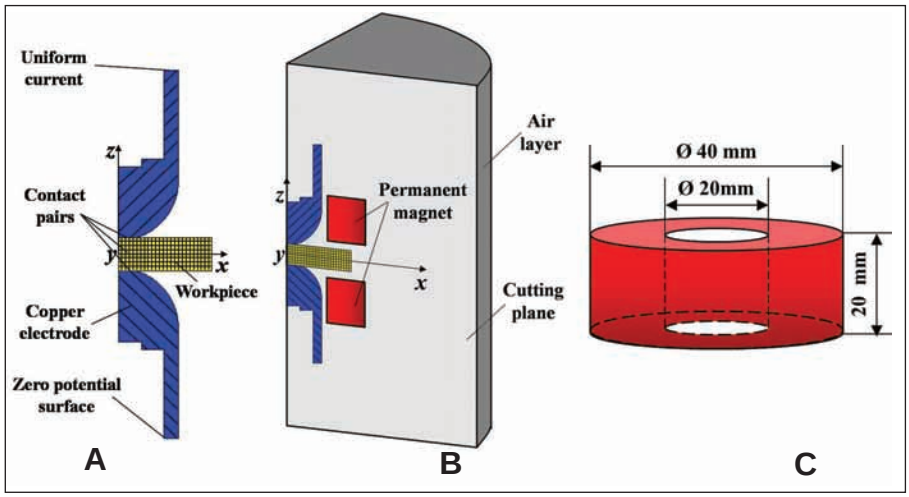

Fig. 1 — Electromagnetic calculation model for MA-RSW process. A — 1/2 2D electric submodel; B — 18 deg, 3D magnetic submodel; C — schematic view of the ring-shaped permanent magnet.

Table 1 — Magnetic Properties of NdFeB Permanent Magnet

Item	Value
Maximum energy product (BH) max/kJ/m^3	287~310
Intrinsic coercive field HcB/kA/m	≥907
Remanent magnetism Br/T	1.22~1.25
Working temperature Tw/°C	≤150

Table 2 — Chemical Composition of Sample Material

Type	Chemical composition in mass %					
	C	Si	Mn	P	S	Al
DP980	0.150	0.500	1.500	0.010	0.002	0.040

For the 2D electric field analysis, a uniform welding current and a relative zero electric potential surface were applied, respectively, at the top and at the bottom, as indicated in Fig. 1A. Thermal boundary conditions were defined as heat convection with water inside the electrode and heat convection with air on the outer surface of electrode and sheets, respectively. The sheet-to-sheet and sheet-to-electrode contact resistances were defined on the faying surfaces between the electrode and sheets (Ref. 19). For the 3D magnetic field analysis, the EMF source was surrounded by a finite air layer, as indicated in Fig. 1B. In addition, a flux parallel condition of magnetic potential was set on the outer surfaces of the air layer. In order to reduce model size and improve calculation efficiency, an 18-deg, 3D wedge-shaped model was used, and cyclic symmetry (Ref. 20) boundaries were specified at the two cutting planes. In order to realize the coupling of the 2D electric model and the 3D magnetic model, the 2D axisymmetric electrical analysis was first carried out to output the current density, which would then be loaded into the 3D magnetic model as excitation input to calculate the magnetic field and magnetic force field.

Ring-shaped NdFeB permanent magnets were used as the EMF source. Dimensions and properties of the axially magnetized magnet are shown in Fig. 1C and Table 1, respectively. The 0.80-mm-thick DP980 steel was used in modeling. The corresponding material data were referred from Ref. 21. Electromagnetic properties of the copper electrode and the air surrounding the electrode and workpieces were referred from Ref. 22.

Experimental Setup and FE Model Validation

Materials and dimensions of the workpieces and permanent magnets used in the

Table 3 — Welding Parameters

Type/ thickness (mm)	Tip diameter (mm)	Electrode force (kN)	Welding current (kA)	Time parameters (ms)		
				Squeezing	Welding	Holding
DP980/0.80	5.0	2.6	3.8~7.9	200	110~190	250

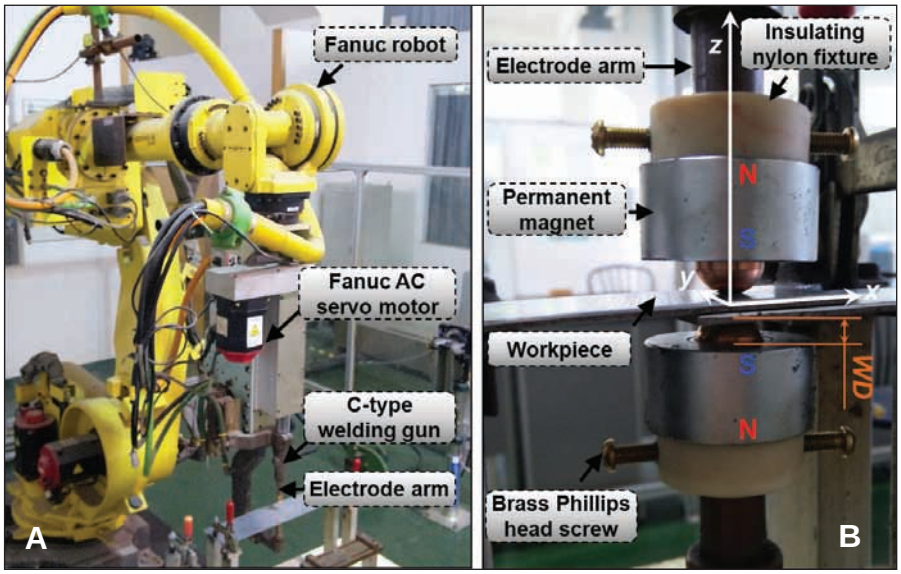

Fig. 2 — MA-RSW equipment. A — RSW system; B — EMF source, N: N pole of the magnet, S: S pole of the magnet; WD*: working distance of the permanent magnet.*

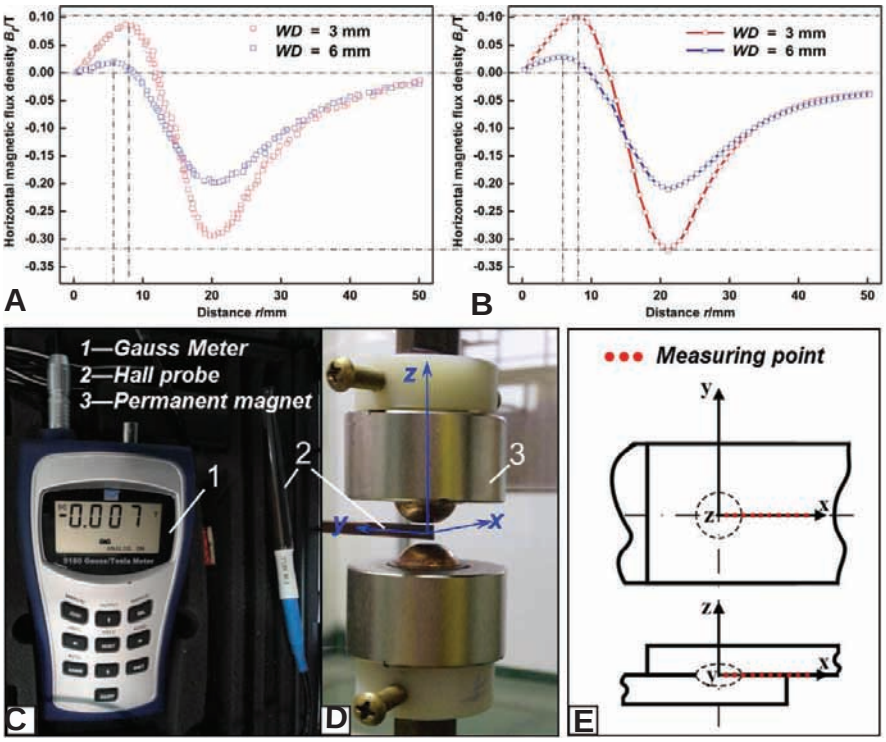

Fig. 3 — Experimental validation of the EMF distribution. A — Experimental results measured by Gauss Meter; B — simulated results; C — Gauss Meter; D — experimental equipment; E — sketch of the measuring path.

experiments were consistent with those used in the numerical simulation. Chemical compositions of DP980 steel and the welding parameters used in this study are listed in Tables 2 and 3, respectively. Figure 2A shows the RSW system, which includes a Fanuc robot R2000-Ib210f with six degrees of freedom, Fanuc AC servo motor α8/4000is, Medar 5000s medium frequency direct current welding controller, and Obara C-type welding gun equipped with two dome-shaped electrodes. The general standard for electrode geometry we referenced is ISO 5821-2009. Specifically, the electrode cap we used was chosen according to Size 2 dome-shaped electrode of General Motors. Chemical composition of the electrode cap is Cr-0.7%, Zr-0.1%, Cu>98.5%. Tip diameter is 5.0 mm.

In the experimental studies on EMF, two modes of EMFs generated by, respectively, a single and a pair of permanent magnets, were both discussed, while for the FE model validation, only the EMF under a pair of permanent magnets was considered. Figure 2B shows the setup of the two magnets. There was an interference fit between a ring-shaped magnet and an insulating nylon fixture, which was then fixed on the electrode arm by three brass Phillips head screws.

According to Lorentz force law, if these two magnets are faced with different poles, the generated magnetic field will be parallel with the welding current, which would hardly produce magnetic force. In the present study, the two magnets were symmetrically located with their south poles (S) against each other. A coordinate origin was set at the intersection point of the electrode central axis and the faying surface of workpieces. Distance from the S pole of a magnet to the tip of the nearest electrode was defined as working distance (*WD*).

In order to verify the accuracy of the FE model, the calculated and measured values of the EMF distributions on the faying surface of workpieces were compared, as shown in Fig. 3. A F. W. BELL 5100 series Gauss Meter connected with a Hall probe was used during the measurement, as shown in Fig. 3C. Since the EMF generated by a pair of permanent magnets was axisymmetric about the center axis of the electrode arm, but also symmetric about the faying surface of workpieces, the horizontal EMF components distributed in the form of concentric circles. A radially oriented measuring path along the x-axis was defined, as shown in Fig. 3E. According to the basic principle of Hall Effect (Ref. 23), the measurement at each point was the average magnetic flux passing through the small square area at the head of the Hall probe. The measurements would be slightly smaller than the real

value. It can be seen in Fig. 3A and B that the measured and calculated distributions of the EMF had a good agreement. The proposed FE model describing the magnetic field distributions during the MA-RSW process was considered to be accurate and reliable, and could be used to calculate the magnetic field and magnetic force distributions during the MA-RSW process.

Results and Discussion

EMF Distribution

As shown in Fig. 4A–C, for a single permanent magnet, the closed magnetic field lines exit from N pole, part of the lines went through the hollow inside, while the rest spread outside around the magnet. Then, all those magnetic field lines gathered near the S pole to go back to the N pole, and completed the closed path. Details within the workpieces were further given in Fig. 4C. It can be seen that the magnetic field in upper and lower sheets under a single permanent magnet was far different, which would induce an unstable fluid flow in the nugget.

For a pair of permanent magnets, as shown in Fig. 4D–F, due to the repulsion of the two faced magnets, the vertical components of the two magnetic fields gradually canceled each other out when closing to the faying surface of the workpieces, whereas the horizontal components superposed with each other. The magnetic field within the workpieces was symmetric about the faying surface under a pair of permanent magnets.

Figure 5 shows the intensity of the horizontal component of the EMF within the workpieces under a single and a pair of permanent magnets, respectively. The maximum (A/A'), minimum (C/C'), and zero (B/B') values of the horizontal component of the EMF flux density on the faying surface of workpieces were dotted in both Fig. 5A and B. Since the vertical component of the EMF is parallel with the welding current density flowing through the workpieces, they will not interact with each other according to Lorentz force law. Only the horizontal component perpendicular to the electrode arm will be taken into account while discussing the effect of the EMF on the weld nugget. It can be seen that because of the superposition of the magnetic field produced by the upper and lower magnets, distributions of the horizontal magnetic field within the workpieces under a pair of magnets were completely symmetric about the faying surface. Moreover, the intensity of the horizontal component of the EMF flux density along the faying surface was twice that under a single magnet.

Figure 6 shows the circumferential external magnetic force distributions along the faying surface. During the practical RSW process, the electromagnetic force will only affect the molten metal inside the nugget, while it has no effect on the solid metal. According to ANSI/AWS/SAE/D8.9-97 (Ref. 24), the minimum acceptable nugget diameter d_c is determined by the following equation:

$$d_c = 4\sqrt{t} = 4\sqrt{0.8} \approx 3.6\,mm \quad (1)$$

where t represents the thickness of steel sheet. Taking account of the variation of welding conditions, the workpieces' center with a 0- to 3.5-mm radius were defined as the welding region, as shown in Fig. 5C. When discussing the effect of the EMF on the weld nugget, only the electromagnetic force within the welding region will be taken into consideration. On the other hand, during the MA-RSW process, two magnetic force components exist in the welding region, including the circumferential external magnetic force and radial induced magnetic force. Since the induced magnet force and its effect on RSW nugget formation have been well studied by Li (Refs. 25, 26) and Wei (Refs. 27, 28), it will not be discussed in the present study. As shown in Fig. 6, the overall trend of the external magnetic force distribution on the faying surface was consistent with that of the horizontal component of the EMF. Intensity of the external magnetic force on the faying surface under a pair of permanent magnets was almost 1.5 times that under a single one. During the MA-RSW process, the circumferential centrifugal movement of the molten metal driven by the electromagnetic force was expected to be more intense under a pair of permanent magnets rather than a single one.

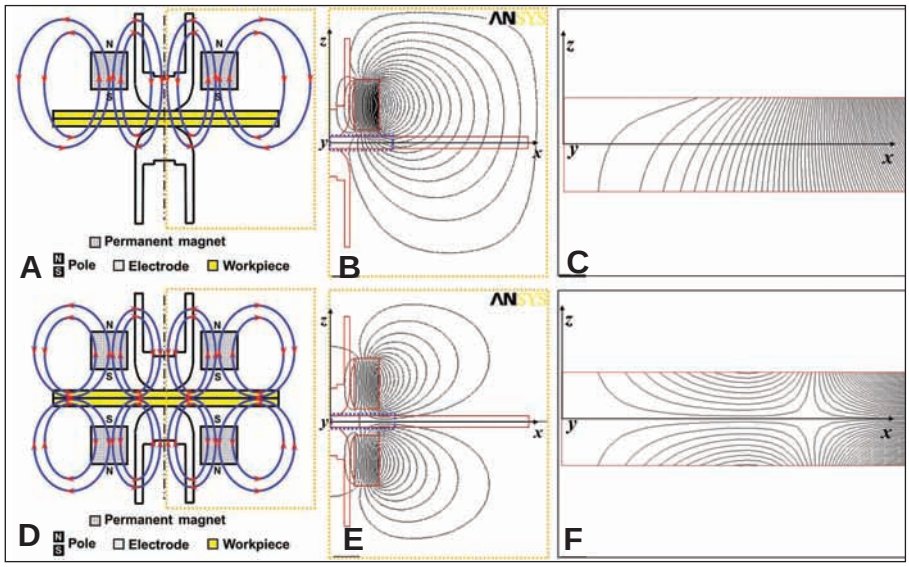

Fig. 4 — EMF distributions under 3-mm WD. *A to C — Under a single magnet; D and F under a pair of magnets; A and D schematic view of the overall EMF distribution; B and E simulated EMF equipotential lines in the region outlined by the orange broken lines shown in A and D, respectively; C and F detailed view of the region outlined by the blue broken lines shown in B and E, respectively.*

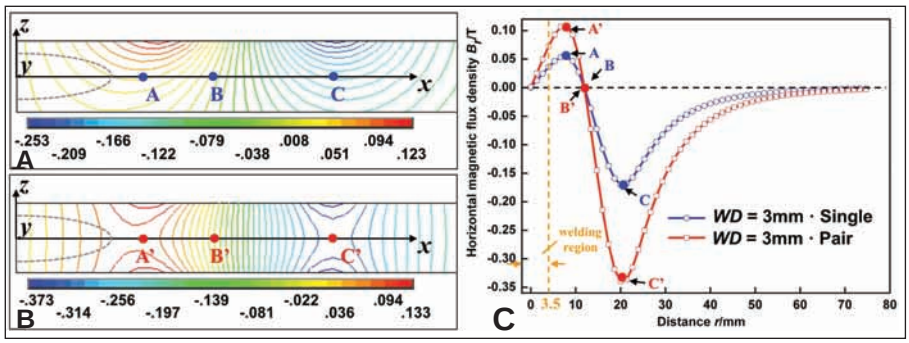

Fig. 5 — Intensity of the horizontal component of the EMF within the workpieces under 3-mm WD. *A and B — Contours of horizontal components of the EMF flux density under a single and a pair of magnets, respectively (unit: Tesla); C — intensity of the horizontal component of the EMF flux density along the x-axis.*

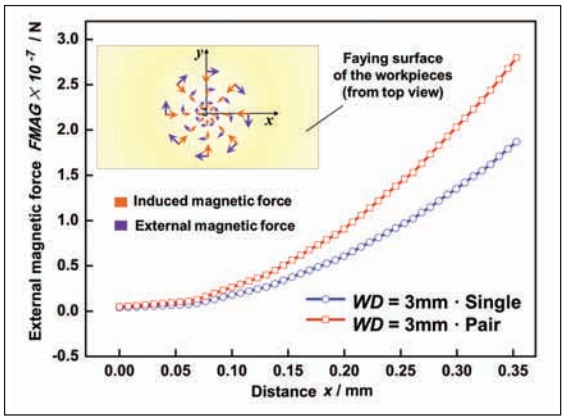

*Fig. 6 — External magnetic force distributions along the x-axis under a single and a pair of permanent magnets, respectively (*WD*, 3 mm).*

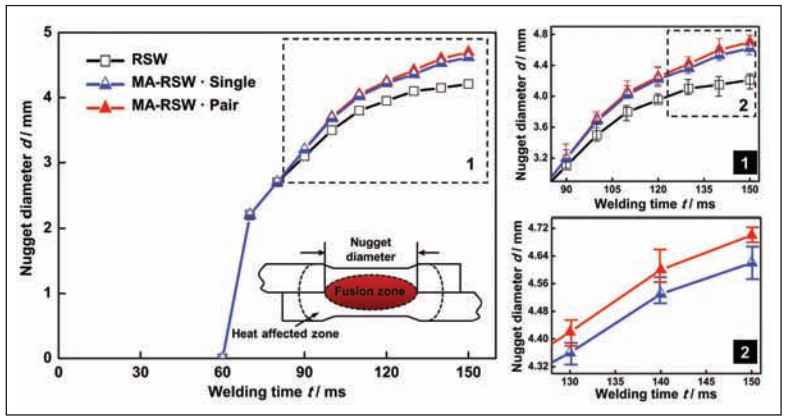

Fig. 7 — Nugget diameter growth process along with the welding time (welding current, 6.0 kA; welding time, 150 ms; WD*, 3 mm).*

Effect of EMF Mode on Nugget Formation

When measuring the size of the growing nugget, two attributes, namely nugget diameter and nugget thickness, were mainly paid attention to in the present study. Usually, width and central thickness of the weld fusion zone is considered as nugget diameter and nugget thickness, respectively. In many cases, the nugget diameter is used as the sole parameter to describe the quality of a spot weld. This is because, when two sheets are joined by a weld at the nugget, its size determines the area of adhesion (Refs. 12, 29) and the stress distribution in the weld nugget interface and its circumference (Ref. 30). On the other hand, requirements on penetration rate (i.e., the ratio of nugget thickness and workpieces) go from 20 to 90% depending on the materials and thickness of workpieces (Ref. 12). There are many studies on the relationship between nugget diameter and weld strength or the type of weld fracture. Results showed that increasing the nugget diameter will enhance weld strength (Refs. 30–32) and raise the probability of button-pullout fracture (Refs. 13, 32).

Nugget formation of the MA welds under different EMFs was presented in curves in Fig. 7. Welding current and welding time were set to 6.0 kA and 150 ms, respectively. Data of a traditional weld under identical welding parameters are also shown as a benchmark. Five repeated experiments were done for each parameter combination to get the errors.

It can be seen that at the early stage of nugget formation, the nugget size of the three types of welds was almost the same. Started from approximately 90 ms, the nugget diameters of these two types of MA welds were both wider than that of the traditional weld, and such difference gradually became more obvious with the heat accumulation in the middle-late welding stage. Moreover, the diameter growth rate of the MA weld under a pair of permanent magnets was faster than that under a single one, especially in the late welding stage. Since the circumferential external magnetic force increased almost monotonically with the increase in the distance from the center to the edge of the welding region shown in Fig. 6, the circumferential stirring effect was expected to be more intense along with the radial expansion of the fusion zone. During the middle-late welding stage, more molten metal would be brought to the edge of the growing nugget driven by the external magnetic force so as to further promote the nugget diameter growth. Moreover, for these two types of MA welds, since the external magnetic force generated by a pair of magnets was stronger, the diameter growth rate of the weld was correspondingly faster.

Figure 8 shows the metallographic views of the nuggets after 150 ms of welding time. Affected by the EMF, the nugget diameter obtained under a single and a pair of permanent magnets was increased by 9.7 and 11.6%, respectively. In addition, differing from the ellipsoidal nugget of the traditional weld, the two types of nuggets of MA weld were both peanut-shell-shaped with the edge thicker than the middle, as shown in Fig. 8B and C.

Such difference in nugget shape could be explained by the flow modes of the molten metal driven by the Lorentz force. In the traditional RSW process, the molten metal driven by the radial induced magnetic force only makes regular rotational flow in four symmetrical loops within the radial planes through the center axis of electrodes (Refs. 25, 26). Led by the radial flow, the high-temperature molten metal in the nugget center would be brought to the edge of the nugget, which would heat the edge region up and is also able to widen the nugget. While in the MA-RSW process, the molten metal driven by the resultant magnetic force would flow not only radially, but also circumferentially. As a result of the centrifugal flow, more heat would be brought from center to the edge of the growing nugget, and the nugget would be decreased in central thickness. On the other hand, in view that the stirring effect near the edge of the faying surface is much stronger than that in the nugget center, a large pressure gradient will form inside the growing nugget along the width direction. Since the molten metal is constrained by the surrounding unmelted solid metal, it would move upward and downward near the nugget edge, which would further widen and especially be capable of thickening the nugget around the edge area.

Besides, for these two types of MA welds, as more heat in the center of the growing nugget under a pair of permanent magnets was taken away, the central thickness of the formed nugget under a pair of magnets would be further decreased. As all the nuggets of the MA weld were peanut-shell-shaped, the commonly acknowledged nugget thickness almost refers to the thinnest place of the nugget, whereas it refers to the thickest place of the nugget of the traditional weld. There was not much sense to compare the absolute value of nugget thickness between the traditional weld and MA weld as long as the penetration rate was in the acceptable range defined by traditional quality evaluation standards.

By comparing the overall shape of the two MA welds shown in Fig. 8B and C, it can be seen that the symmetry of the nugget under a single permanent magnet was relatively poorer. Two ends of the nugget shifted upward slightly. Such nugget offset is usually not preferred when welding two sheets with equal thickness. However, the asymmetric EMF may provide another way to improve the nugget offset in welding multistackup sheets with

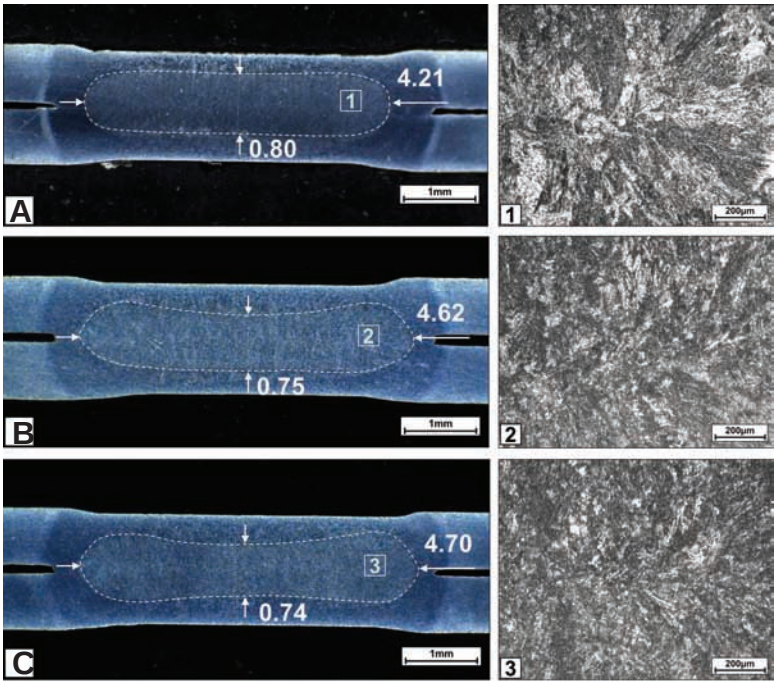

Fig. 8 — Typical cross-sectioned weld nugget and the microstructures in the weld nugget. A — Traditional weld; B — MA weld under a single permanent magnet; C — MA weld under a pair of permanent magnets (welding current, 6.0 kA; welding time, 150 ms; WD*, 3 mm).*

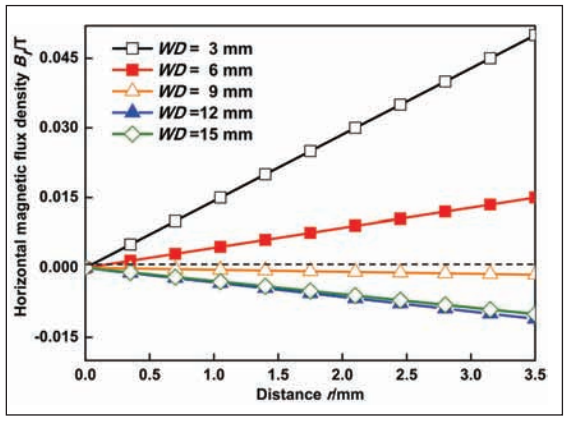

Fig. 9 — Intensity of the horizontal component of the EMF under a pair of permanent magnets along the x-axis in the 0- to 3.5-mm radius welding region.

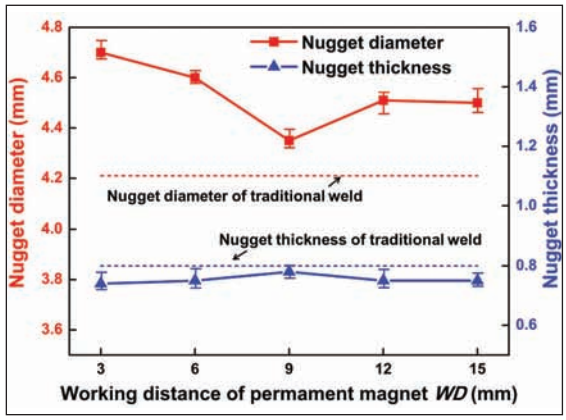

Fig. 10 — Nugget size variations of the MA welds under a pair of permanent magnets along with the changes in WD *(welding current, 6.0 kA; welding time, 150 ms).*

different thickness (Refs. 33, 34).

The difference in EMF mode not only changes the nugget shape, but also affects the microstructures within the nugget. As shown in Fig. 8, the macrocrystallization directions in the two MA welds were both less obvious compared with that of the traditional weld. Moreover, under a pair of permanent magnets, the oriented growth of the dendrites toward the faying surface was less directional, and the boundary of the faying surface was also less visible.

Therefore, compared with the MA weld under a single magnet, the MA weld under a pair of magnets has exhibited better quality in view of nugget symmetry, nugget diameter, and nugget microstructures. The following discussions on nugget size variations under different *WD*s were all based on the symmetric EMF generated by a pair of permanent magnets.

Effect of EMF Intensity on Nugget Size

Intensity of the EMF can be adjusted by changing *WD*. Variations of the horizontal component of the EMF flux density along the x-axis of the 0- to 3.5-mm radius welding region under different *WD*s were described in Fig. 9 based on the present FE model.

Intensity of the horizontal component of the EMF increased monotonically from the center to the edge of the welding region. Besides, along with the increase in *WD*, the slope of the curves became smaller due to the weakening of the repulsion effect between the two magnets. Because of the special ring-shaped structure of the axially magnetized permanent magnets (Ref. 35), the direction of the horizontal magnetic field gradually changed from the positive x-axis oriented to the negative x-axis oriented along with the *WD* varying from 3 to 15 mm. Since the horizontal component of the EMF was always perpendicular to the electrode arm, it did not matter whether the measurements were positive or negative. Specifically, when *WD* was set to 3 mm, the horizontal component was the strongest; when *WD* was set to 6, 12, and 15 mm, it was weaker; when *WD* was set to 9 mm, intensity of the horizontal component was close to zero.

Figure 10 shows the nugget size variations of the MA weld along with the changes in *WD*. Data of a traditional weld under identical welding parameters were also plotted in broken lines as a benchmark. It can be seen that when the horizontal component of the EMF was the strongest under 3-mm *WD*, the nugget of the MA weld was the widest and thinnest. By contrast, when the horizontal component was the weakest under 9-mm *WD*, the nugget of the MA weld was the narrowest and thickest. Moreover, compared with the nugget thickness, the nugget diameter was more sensitive to the variations of EMF intensity. Since the nugget diameter is well acknowledged as the major criteria when evaluating the quality of a RSW weld, it is acceptable to suggest that the stronger the horizontal component of the EMF within the welding region is, the better the weld quality will be. However, as the nuggets of MA weld were all peanut-shell shaped, the central thickness should probably be considered as an important evaluation criteria, too, even if the penetration rate is within the acceptable range. Because the stress distributions within the peanut-shell-shaped nugget under external loads might greatly differ from that within the ellipsoidal nugget.

Sensitivity of the MA-RSW Process to Welding Current

During the practical MA-RSW process, current density not only determines the total heat input, but also greatly affects the intensity of the electromagnetic stirring force. Sensitivity of the MA-RSW process to the welding current was dis-

Table 4 — Comparison of Mechanical Performance of Traditional Welds and MA Welds Along with the Variation of Welding Current (welding time: 150 ms; *WD*: 3 mm)

	RSW			MA-RSW		
Current (kA)	TSF (kN)	Displacement at failure (mm)	Failure mode*	TSF (kN)	Displacement at failure (mm)	Failure mode*
6.0	9.01	1.45	C	9.61	1.59	C
	9.06	1.43	C	9.68	1.62	C
	8.94	1.47	C	9.63	1.58	C
	9.07	1.52	C	9.55	1.56	C
	9.03	1.47	C	9.62	1.50	C
Average	9.02	1.47	100% C	9.62	1.57	100% C
Increase Rate	–	–	–	+6.61%	+6.95%	0%
5.6	8.42	1.40	B	9.10	1.57	C
	8.70	1.49	C	9.17	1.64	C
	8.32	1.39	B	9.06	1.49	C
	8.53	1.37	B	8.90	1.53	B
	8.38	1.30	B	9.18	1.52	C
Average	8.47	1.39	80% B + 20% C	9.08	1.55	20% B + 80% C
Increase Rate	–	–	–	+7.23%	+11.51%	+ 60% C
5.1	7.56	1.03	A	8.63	1.37	B
	8.21	1.19	B	8.65	1.41	B
	7.77	1.10	A	8.51	1.33	B
	7.43	0.97	A	8.43	1.30	B
	8.03	1.10	A	8.77	1.38	B
Average	7.80	1.08	80% A + 20% B	8.60	1.36	100% B
Increase Rate	–	–	–	+10.23%	+25.97%	+80% B

*A — interfacial fracture; B — button-pullout fracture; C — strong button-pullout fracture.

cussed by tensile-shear testing on the traditional welds and MA welds under different welding currents. Detailed experimental results are presented in Table 4 with the average value and increase rate listed.

As to the fracture mode, commonly acknowledged definitions of three typical fracture modes were referred in the present study. For typical interfacial fracture (represented by A in Table 4), full separation of the faying surface of workpieces occurs as a result of fracture through the weld; for typical button-pullout failure, the fracture develops along the periphery of the weld (Ref. 36). More specifically, the button-pullout fracture can be further divided into two modes according to the fracture development path (Ref. 6). For a strong weld (represented by B in Table 4), button-pullout fracture develops within both the base metal and heat-affected zone, and a hole is left in one of the steel sheets; for an extremely strong weld (represented by C in Table 4), a button-pullout fracture develops only within the base metal, and a hole is left in each of the steel sheets.

It can be seen that as a result of the increase in nugget diameter shown in Fig. 8, the tensile-shear strength and elongation at break of the MA welds were respectively stronger and higher than that of the traditional ones. What's more, the improvement of weld strength and ductility was more obvious for welds under relatively low welding current, whereas it was less obvious for welds under relatively high welding current.

Such phenomena could be explained by the differences in fracture modes under different welding currents. With less heat input under relatively low welding currents, a small weld was formed with a high risk of interfacial fracture under external loads. In view of the fracture development path under interfacial fracture, it can be inferred that the mechanical performance of a small weld heavily depends on nugget appearance. The increase in nugget diameter and refinement of solidified microstructures would lead to the relatively obvious improvement of weld strength and ductility. By contrast, with more heat input under relatively high welding current, a big weld was formed with high probability of button-pullout fracture, of which the failure loads and elongations depends on not only weld quality, but also the property of base metal. The improvement of weld mechanical performance due to nugget diameter increase was relatively less obvious.

Differences in the fracture modes between the traditional welds and MA welds could be explained more clearly by referring to the typical load versus displacement curves of welds under different welding currents shown in Fig. 11. It can be inferred that affected by the EMF, the probability of weld button-pullout fracture for DP980 steel was raised, which indicated the enhancement of energy absorption capacity under impact loading, especially under low welding current.

However, taking account of the fact that compared with the traditional welds, the peanut-shell-shaped MA welds were not only wider, but also thinner, such difference became more obvious along with the increase in the EMF intensity. With the variations of the EMF, there might be a critical value for the ratio of diameter increase and thickness decrease, less than which the EMF would have negative effect on weld strength. More specific and systematic studies should be carried out in the future to investigate the effectiveness of the EMF on weld mechanical performance improvement.

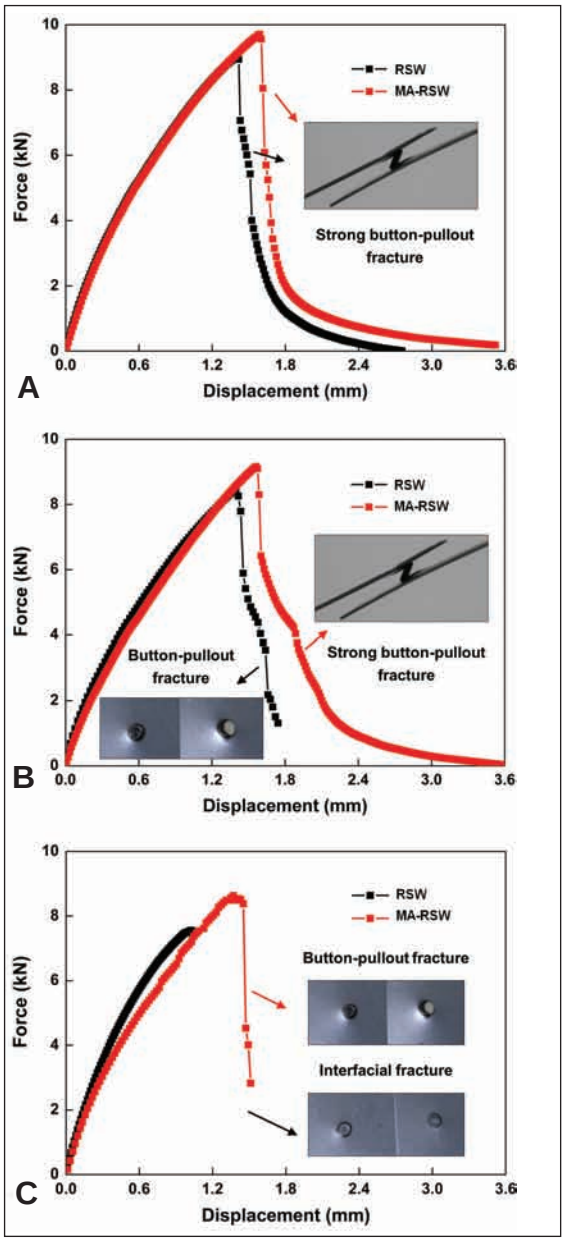

Fig. 11 — Typical load vs. displacement curves and the corresponding fracture modes of welds under different welding currents. A — 6.0 kA; B — 5.6 kA; C — 5.1 kA (welding time, 150 ms; WD*, 3 mm).*

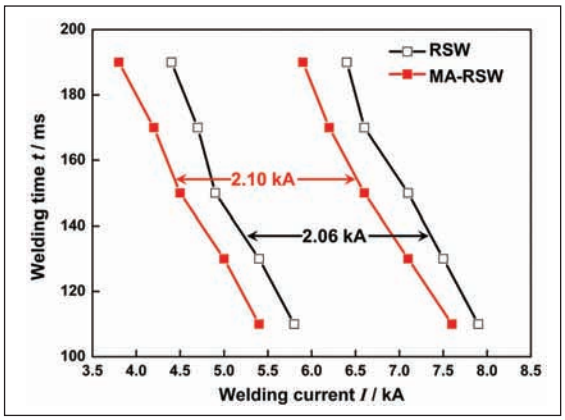

*Fig. 12 — Comparison of weld lobe diagram between the traditional RSW and MA-RSW process (*WD*, 3 mm).*

Weldability of MA-RSW Process

In order to further investigate the practicality of the MA-RSW process, a comparative study on weld lobe diagram between the traditional RSW and MA-RSW process was conducted. Results are shown in Fig. 12. The left boundary of weld lobe diagram was determined by the minimum nugget diameter, which was about 3.6 mm according to Equation 1. The right boundary of weld lobe diagram was determined by the threshold value of welding current; beyond that, expulsion will occur.

It can be seen that affected by the EMF, the right boundary of the weld lobe diagram of the MA-RSW process moved leftward by nearly 400 A. Due to the strong fluid flow driven by the circumferential magnetic force, a lot of high-temperature molten metal would rush to the edge of the growing nugget, which could induce expulsion during the MA-RSW process, especially in the case of high welding current and long welding time. Such phenomena should be considered as a negative aspect of the MA-RSW process from the practical point of view. On the other hand, due to the increase in nugget diameter, the left boundary of the weld lobe diagram of the MA-RSW process also moved leftward by approximately 400 A. The overall width of the weld lobe diagram remained almost unchanged. Those results indicated that under proper welding parameters, the MA-RSW process could be an alternative way to guarantee weld quality as well as reduce energy consumption.

Conclusions

The present study systematically analyzed the mode and intensity of an externally applied constant magnetic field and its effect on nugget formation during the magnetically assisted resistance spot welding of 0.80-mm-thick DP980 steel. Concerning the practical application, sensitivity of the external magnetic field on welding current was discussed. The effect of the external magnetic field on the weld lobe diagram was also investigated.

The following conclusions were drawn:

1. Intensity of the horizontal component of the external magnetic field increased monotonically from the center to the edge of the 0- to 3.5-mm radius welding region. On the faying surface of the workpieces, the horizontal magnetic flux density and circumferential magnetic force under a symmetric magnetic field generated by a pair of permanent magnets were, respectively, twice and 1.5 times that under an asymmetric one by a single magnet. Moreover, the horizontal magnetic field in the welding region went through a changing process as "weak-strong-weak" along with the increase in the distance between the permanent magnets and workpieces.

2. Growth rate of the nugget diameter for the magnetically assisted weld was faster than that of the traditional weld, especially during the middle-late welding stage. Furthermore, with a symmetric magnetic field applied instead of an asymmetric one, the nugget growth rate was even faster, the diameter was longer, the nugget symmetry was better, and the microstructures in the fusion zone were finer.

3. Magnetically assisted welds were generally peanut-shell shaped with the nugget edges thicker than the middle. What's more, with the increase in the external magnetic field intensity, the nugget became even wider and thinner.

4. Compared with the traditional welds under identical welding parameters, all the magnetically assisted welds exhibited higher tensile-shear strength, stronger energy absorption capacity, and higher probability of button-pullout fracture. Such improvement of mechanical performance was more obvious for welds under relatively low welding current.

5. Affected by the external magnetic field, the weld lobe diagram of resistance spot welded DP980 steel moved leftward for near 400 A, while the width remained unchanged. The magnetically assisted resistance spot welding process could be an alternative method to ensure weld quality and meanwhile reduce energy consumption under proper welding parameters.

Acknowledgment

The authors gratefully acknowledge the support of the National Natural Science Foundation of China under Grant No. 50705059.

References

1. Lopez-Cortez, V. H., and Reyes-

Valdes, F. A. 2008. Understanding resistance spot welding of advanced high-strength steels. *Welding Journal* 87(12): 36-s to 40-s.

2. Tumuluru, M. D. 2006. Resistance spot welding of coated high-strength dual-phase steels. *Welding Journal* 85(8): 31-s to 37-s.

3. Chuko, W. L., and Gould, J. E. 2002. Development of appropriate resistance spot welding practice for transformation-hardened steels. *Welding Journal* 81(1): 1-s to 8-s.

4. Gould, J. E., Khurana, S. P., and Li, T. 2006. Predictions of microstructures when welding automotive advanced high-strength steels. *Welding Journal* 85(1): 111-s to 116-s.

5. Khan, M. I., Kuntz, M. L., Biro, E., and Zhou, Y. 2008. Microstructure and mechanical properties of resistance spot welded advanced high strength steels. *Materials Transactions* 49(7): 1629-s to 1637-s.

6. Marya, M., Wang, K., Hector, L. G., et al. 2006. Tensile-shear forces and fracture modes in single and multiple weld specimens in dual-phase steels. *ASME Journal of Manufacturing Science and Engineering* 128(1): 287-s to 298-s.

7. Combescure, A., Delcroix, F., Caplain, L., et al. 2003. A finite element to simulate the failure of weld points on impact. *International Journal of Impact Engineering* 28: 783-s to 802-s.

8. Zhou, M., Hu, S. J., and Zhang, H. 1999. Critical specimen sizes for tensile-shear testing of steel sheets. *Welding Journal* 78(9): 305-s to 312-s.

9. Baltazar Hernandez, V. H., Kuntz, M. L., Khan, M. I., et al. 2008. Influence of microstructure and weld size on the mechanical behaviour of dissimilar AHSS resistance spot welds. *Science and Technology of Welding and Joining* 13(8): 769-s to 776-s.

10. Peterson, W. 2006. Methods to minimize the occurrence of interfacial fractures in HSS spot welds. *Sheet Metal Welding Conference X*.

11. GM/NAO. 1996. *High Strength Steel Applications Manual*. Chapter 2, high strength steel versus mild steel: 2-s to 60-s.

12. Zhang, H., and Senkara, J. 2005. *Resistance Welding Fundamentals and Applications*. CRC Press/Taylor & Francis Group, Boca Raton, London, New York.

13. Marya, M., and Gayden, X. Q. 2005. Development of requirements for resistance spot welding dual-phase (DP600) steels. Part 2: Statistical analyses and process maps. *Welding Journal* 84(12): 197-s to 207-s.

14. Oh, K. S., and Chang, Y. W. 1995. Macrosegregation behavior in continuously cast high carbon steel blooms and billets at the final stage of solidification in combination stirring. *ISIJ International* 35(7): 866-s to 875-s.

15. Luo, J., Luo, Q., Lin, Y. H., et al. 2003. A new approach for fluid flow model in gas tungsten arc weld pool using longitudinal electromagnetic control. *Welding Journal* 82(8): 202-s to 206-s.

16. Li, Y. B., Shen, Q., Lin, Z. Q., et al. 2011. Quality improvement in resistance spot weld of advanced high strength steel using external magnetic field. *Science and Technology of Welding and Joining* 16(5): 465-s to 469-s.

17. Shen, Q., Li, Y. B., Lin, Z. Q., et al. 2011. Impact of external magnetic field on weld quality of resistance spot welding. *ASME Journal of Manufacturing Science and Engineering* 133(5): 15001-1-s to 15001-7-s.

18. Shen, Q., Li, Y. B., Lin, Z. Q., et al. 2011. Effect of external constant magnetic field on weld nugget of resistance spot welded dual-phase steel DP590. *IEEE Transactions on Magnetics* 47(10): 4116-s to 4119-s.

19. Rogeona, P., Carrea, P., Costaa, J., et al. 2008. Characterization of electrical contact conditions in spot welding assemblies. *Journal of Materials Processing Technology* 195(1–3): 117-s to 124-s.

20. ANSYS, 2011. Version 12. Canonsburg: ANSYS Inc.

21. Richard, D., Fafard, M., Lacroix, R., et al. 2003. Carbon to cast iron electrical contact resistance constitutive model for finite element analysis. *Journal of Materials Processing Technology* 132(1–3): 119-s to 131-s.

22. Tsai, C. L., Dai, W. L., Dickinson, D. W., et al. 1991. Analysis and development of a real time control methodology in resistance spot welding. *Welding Journal* 70(12): 339-s to 351-s.

23. Edward Ramsden. 2006. *Hall-effect sensors: theory and applications*. Newnes, Burlington.

24. ANSI/AWS/SAE/D8.9–97, Section 6.7. American National Standard. 1997. Weld button criteria, recommended practices for test methods for evaluating the resistance spot welding behavior of automotive sheet steel materials.

25. Li, Y. B., Lin, Z. Q., Shen, Q., et al. 2011. Numerical analysis of transport phenomena in resistance spot welding process. *ASME Journal of Manufacturing Science and Engineering* 133(9): 031019-1-s to 031019-8-s.

26. Li, Y. B., Lin, Z. Q., Hu, S. J., et al. 2007. Numerical analysis of magnetic fluid dynamics behaviors during resistance spot welding. *Journal of Applied Physics* 101(5): 053506-1-s to 053506-10-s.

27. Wei, P. S., and Wu, T. H. 2011. Magnetic property effect on transport processes in resistance spot welding. *Journal of Physics D: Applied Physics* 44: 325501-1-s to 325501-10-s.

28. Wei, P. S., Wu, T. H., and Hsieh, S. S. 2011. Phase change effects on transport processes in resistance spot welding. *Journal of Mechanics* 27(1): 19-s to 26-s.

29. Zhou, M., Zhang, H., and Hu, S. J. 2003. Relationships between quality and attributes of spot welds. *Welding Journal* 82(4): 72-s to 77-s.

30. Pouranvari, M., Asgari, H. R., Mosavizadch, S. M., et al. 2007. Effect of weld nugget size on overload failure mode of resistance spot welds. *Science and Technology of Welding and Joining* 12(3): 217-s to 225-s.

31. Tumuluru, M. D. 2006. Resistance spot welding of coated high-strength dual-phase steels. *Welding Journal* 85(8): 31-s to 37-s.

32. Pouranvari, M., and Marashi, S. P. H. 2010. Factors affecting mechanical properties of resistance spot welds. *Materials Science and Technology* 26(9): 1137-s to 1144-s.

33. Ma, N., and Murakawa, H. 2010. Numerical and experimental study on nugget formation in resistance spot welding for three pieces of high strength steel sheets. *Journal of Materials Processing Technology* 210(14): 2045-s to 2052-s.

34. Nielsen, C. V., Friis, K. S., Zhang, W., et al. 2010. Three-sheet spot welding of advanced high-strength steels. *Welding Journal* 90(2): 32-s to 40-s.

35. Edward, M. 1986. *Electricity and Magnetism*. Berkeley Physics Course, Non Basic Stock Line.

36. Marya, M., and Gayden, X. 2005. Development of requirements for resistance spot welding of dual-phase steels (DP600) — Part I: The causes of interfacial fractures. *Welding Journal* 84(11): 172-s to 182-s.